### **ORIGINAL ARTICLE**



# Environmental characterisation and stabilisation of a $2 \times 200$ -meter outdoor fibre interferometer at the CHARA Array

Lucien Lehmann<sup>1</sup> • Laurent Delage<sup>1</sup> · Ludovic Grossard<sup>1</sup> · Francois Reynaud<sup>1</sup> · Steve Golden<sup>2</sup> · Craig Woods<sup>2</sup> · Larry Webster<sup>2</sup> · Judit Sturmann<sup>2</sup> · Theo ten Brummelaar<sup>2</sup>

Received: 23 April 2018 / Accepted: 1 April 2019 / Published online: 1 May 2019 © Springer Nature B.V. 2019

### **Abstract**

In the framework of the ALOHA project (Astronomical Light Optical Hybrid Analysis), devoted to high resolution imaging in the L band, we investigate in this paper the possibility to deploy fibre links between the telescopes of the CHARA Array. As a first step, we set up an outdoor hectometric fibre interferometer to measure the vibration environment at the Mount Wilson Observatory. The optical path difference of this interferometer has been actively stabilised within an accuracy better than 4  $nm_{RMS}$ , a stability largely sufficient for any interferometric application.

**Keywords** Interferometry · Optical fibre · Long baseline · Servo control · High resolution imaging

### 1 Introduction

In the last decade, the use of optical fibre has been widespread among the astronomical community through interferometer projects like JouFLU [1], AMBER [2], MIRC [3] or GRAVITY [4]. Optical fibres show a lot of advantages in terms of spatial filtering [5], high throughput and implementation versatility. However, optical fibres have not yet been used for very long-distance coherent light transport in the context of an astronomical interferometer. Some early works have been done (OHANA Keck [6], OHANA Iki [7]) but never reaching a hectometric or kilometric baseline, due to the lack of active fibre length stabilisation.



 <sup>□</sup> Lucien Lehmann
 □ Lucien.lehmann@xlim.fr

<sup>1</sup> XLIM, 123 rue A. Thomas, 87060 Limoges, France

<sup>&</sup>lt;sup>2</sup> The CHARA Array, Mt. Wilson Observatory, Mt. Wilson, CA 91023, USA

The experiment reported in this paper is a part of the long term ALOHA project (Astronomical Light Optical Hybrid Analysis) schematically represented in Fig. 1. The goal of this project is to adapt the optical spectral domain of the astronomical source to the operating spectrum of commercial fibres. For this purpose, a non-linear optical process converts mid-infrared light to a spectral domain compatible with single mode silica optical fibre. This conversion is performed at each telescope, so that the converted light can be transported through optical fibres over very long paths. So, the ALOHA concept could give the opportunity to implement a ground-based interferometer array in the mid or far infrared domain in order to observe challenging science cases such as protoplanetary disks or Active Galactic Nuclei [8].

The Georgia State University Center for High Angular Resolution Astronomy (CHARA) Array is an optical/near infrared interferometer with the longest baseline available [9]. This instrument on the grounds of the Mount Wilson Observatory in California comprised of an array of six 1-meter telescopes with baselines ranging from 34 to 330 m. The CHARA Array routinely provides astronomical data in the visible and near infrared domains (up to the astronomical K band). Our mid-term objective is to set up ALOHA on the CHARA Array in order to allow the study of the astronomical L band. The non-linear conversion from 3.39  $\mu$ m to 810 nm and fringe contrast measurement have already been demonstrated in laboratory experiments [10] as well as the multichannel spectral mode of the instrument in the H band [11]. However, the specific requirements to reach a sub-wavelength optical path stability for fibre links between the CHARA Array telescopes have not been investigated yet. In this paper we present the implementation of an outdoor hectometric

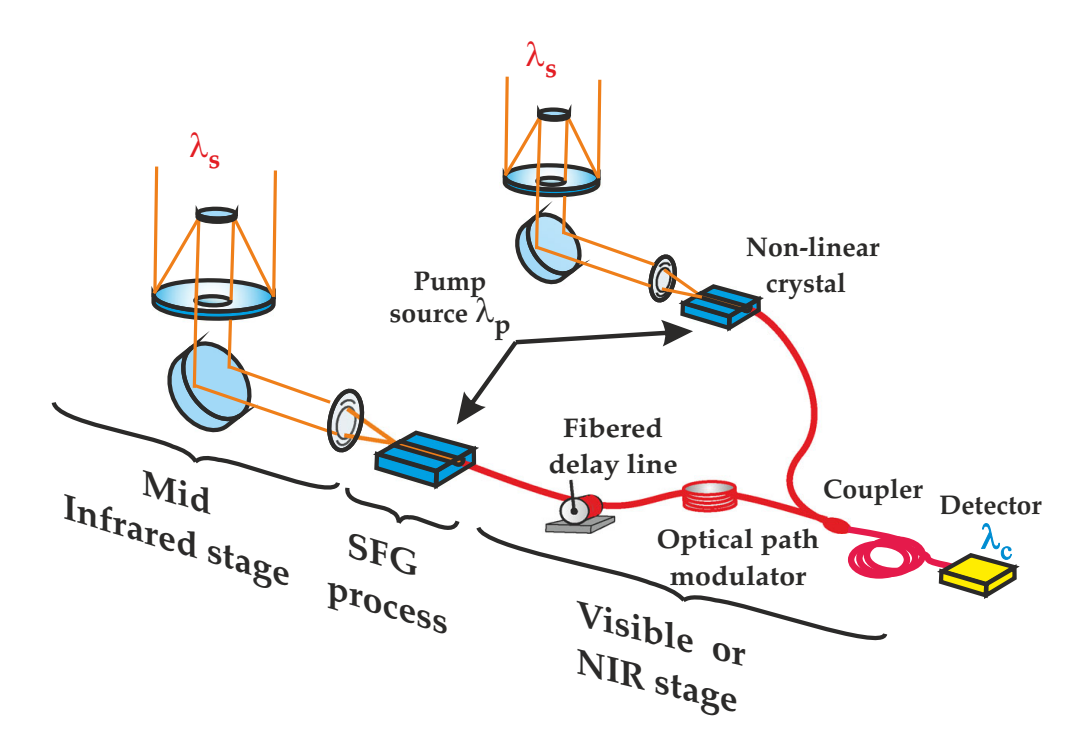


Fig. 1 Schematic of the ALOHA interferometer with two telescopes. Powered by a pump source at  $\lambda_p$ , the infrared signal at  $\lambda_s$  coming from the stellar object is up converted to the visible or near infrared wavelength  $\lambda_c$  by sum frequency generation (SFG) in a non-linear crystal



fibre interferometer at the Mount Wilson Observatory as a precursor of a future fibre linkage. This experiment focused on the impact of the thermal and vibrational environment on the Optical Path Difference (OPD) of the instrument. We deployed two 200-meter long optical cables between the CHARA recombination laboratory and the East-2 (E2) telescope. We measured the long-term drift of the OPD as a function of time and stabilised this OPD with great accuracy. Both tasks were accomplished by an active control of the OPD of the interferometer.

The experimental setup is presented in Section 2. Section 3 details the data processing used to retrieve both the amplitude of the OPD drift and the stability OPD when the servo loop is closed. The results of this experiment are presented in Section 4.

# 2 The experimental setup

The fibre interferometer was set up at the CHARA Array as shown in Fig. 2. The setup most importantly included two 200-meter single mode and polarisation maintaining optical fibres that were laid down between the recombination laboratory and the E2 telescope in a Mach-Zehnder configuration. Over the 160-meter distance of the telescope and the lab there were two 40-meter sections remaining in each optical cable. These sections were spread around the telescope apart from each other to generate 2x40 m of non common paths. These non common paths were comparable with the two shortest baselines of the CHARA Array: the S1–S2 baseline (34 m) and E1–E2 baseline (66 m). The optical cables were laid directly on the ground and packed

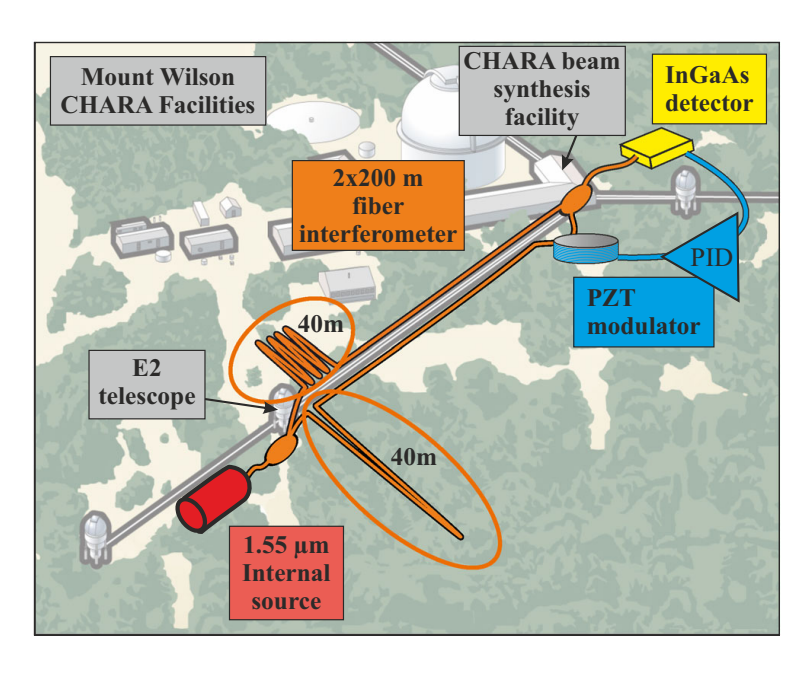


**Fig. 2** Mach-Zehnder interferometer setup at the Mount Wilson Observatory. An internal source is split between two 200 m single mode polarisation-maintaining fibre and recombined by two fibre couplers. The interferometric signal, detected by an InGaAs detector, is used to measure and control the OPD variation of the interferometer through a PID regulator



into cylindrical foam pieces to damp vibrations and limit thermal fluctuations. This very basic passive isolation could be significantly improved in the future.

At the fibre tips close to the E2 telescope, the polarised field of the light emitted by a 1.55  $\mu$ m distributed feedback (DFB) laser was split by a 50/50 polarisation maintaining fibre coupler and fed the two arms of the interferometer. The light was recombined by a second and identical fibre coupler at the outputs of the fibred arms, located inside the "Beam Synthesis facility". The interferometric signal detected by an InGaAs photodiode was used to drive a servo loop that controlled the OPD of the interferometer. The actuator of this servo control was a fibre stretcher comprising a cylindrical piezoelectric ceramic (PZT) on which 2 m of one of the fibre-arm was coiled. A driving voltage allowed controlling the OPD with a full stroke of 150  $\mu$ m. Considering that the coherence length of the DFB source is around 200 m, we could assume the laser to be monochromatic for our purposes since the fibre-arm lengths were matched within 10 cm. In addition, thermal regulation of the laser diode ensured the stability of the emitted wavelength. Under these experimental conditions, the variations of the detected interferometric signal depended only on the drift of the OPD.

## 3 Method

Figure 3 shows the block diagram of the servo loop used to control the OPD of the interferometer and measure its variations. The detector produces a voltage *V* proportional to the intensity of the interferometric signal. It can be written as:

$$V = V_0 \left[ 1 + \cos \left( \frac{2\pi \delta}{\lambda} \right) \right], \tag{1}$$

$$V_{\text{set}} = V_0$$

$$V_{\text{set}} = V_0$$

$$V_{\text{corr}} = V_0$$

$$V_{\text{corr}} = V_0$$

$$V_{\text{corr}} = V_0$$

$$V_{\text{env}} = V_0$$

$$V_{\text{offibre0}} = V_0$$

$$V = V_0 (1 + \cos(2\pi\delta/\lambda))$$

$$\delta = \delta_{\text{corr}} + \delta_{\text{env}} + \delta_{\text{fibre0}}$$

Fig. 3 Block diagram of the servo loop. The interferometric signal V is compared to a set point  $V_{\text{set}}$ . The PID regulator processed the error signal  $\varepsilon$  in order to control the OPD of the interferometer. DET: InGaAs detector; HV amp: high voltage amplifier; PZT: piezoelectric actuator



where  $V_0$  is the mean value of the interferometric signal,  $\lambda$  is the wavelength of the DFB source, and  $\delta$  is the total OPD. The difference between the interferometric signal V and a voltage set-point  $V_{\text{set}}$  generates the error signal  $\varepsilon$  that feeds a proportional-integral-derivative (PID) controller. The PID output signal  $V_{\text{corr}}$  is amplified by a high voltage amplifier. Finally, this amplified PID voltage drives the fibre stretcher and modifies the total OPD  $\delta$  of the interferometer by a value  $\delta_{\text{corr}} = \alpha V_{\text{corr}}$ . We can easily measure  $\alpha$  in open loop by counting the number of fringes produced on  $\varepsilon$  when applying a known ramp voltage to the actuator. In our case,  $\alpha = 5 \, \lambda/V$  corresponding to 7.75  $\mu$ m/V.

We simultaneously record the error signal  $\varepsilon$  and the correction signal  $V_{\rm corr}$  at a sampling rate of 10 kHz per acquisition channel.

As we choose  $V_{\text{set}}$  equal to the mean of the interferometric signal  $V_0$ , the error signal is given by:

$$\varepsilon = V_0 - V_0 \left[ 1 + \cos \left( \frac{2\pi \delta}{\lambda} \right) \right] = V_0 \cos \left( \frac{2\pi \delta}{\lambda} \right) \tag{2}$$

The total OPD  $\delta$  is the sum of three components:  $\delta_{corr}$ , the OPD correction imposed by the fibre stretcher,  $\delta_{env}$ , the optical path drift due to the environmental conditions and  $\delta_{fibre0}$ , the initial and fixed imbalance of the fibre optical paths. In closed loop,  $\delta$  is near to one of the operating points (Fig. 4) and can be expressed as:

$$\delta = k\lambda + \frac{3}{4}\lambda + \Delta\delta \tag{3}$$

where  $k \in \mathbb{Z}$  and  $\Delta \delta$  is the uncorrected OPD. Using (2), the error signal can be written as:

$$\varepsilon = V_0 \cos \left( 2k\pi + \frac{3\pi}{2} + \frac{2\pi \Delta \delta}{\lambda} \right) = V_0 \sin \left( \frac{2\pi \Delta \delta}{\lambda} \right) \tag{4}$$

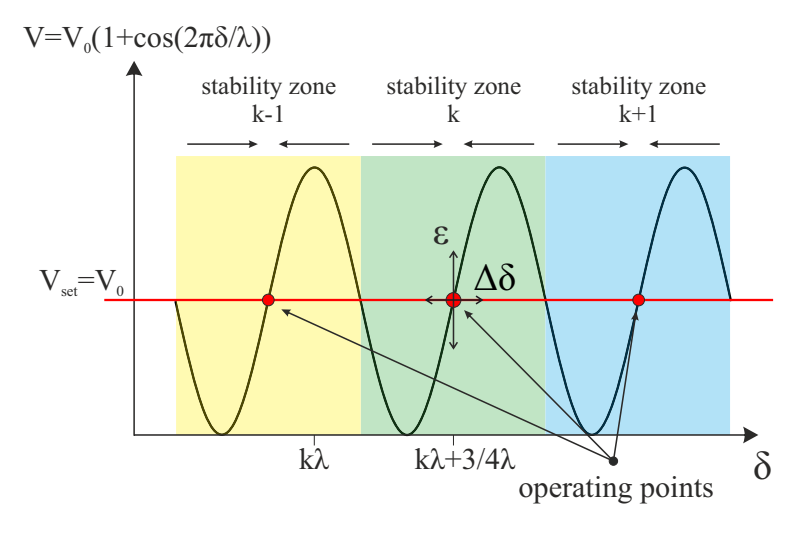


Fig. 4 Interferometric signal V as a function of the OPD  $\delta$ . For a given set point  $V_{\text{set}}$ , multiple operating points are possible. Each operating point is related to an OPD stability zone



In closed loop  $-\pi < 2\pi \Delta \delta/\lambda < \pi$ , so  $\varepsilon$  is a direct measurement of the uncorrected OPD  $\Delta \delta$ :

$$\Delta \delta = \frac{\lambda}{2\pi} \arcsin\left(\frac{\varepsilon}{V_0}\right) \tag{5}$$

We can also deduce the OPD drift due to the environmental conditions  $\delta_{env}$ . Let's consider the total OPD  $\delta$ :

$$\delta = \delta_{\text{env}} + \delta_{\text{corr}} + \delta_{\text{fibre0}} \tag{6}$$

Using (3), we can write:

$$\Delta \delta = \delta_{\text{env}} + \delta_{\text{corr}} + \underbrace{\delta_{\text{fibre0}} - k\lambda - \frac{3}{4}\lambda}_{\delta_0}$$
 (7)

In closed loop  $|\Delta \delta|$  is negligible compared to  $|\delta_{\text{corr}}|$ . So, the command voltage  $V_{\text{corr}}$  is a direct measurement of the optical path drift due to the environmental conditions with an unknown constant offset of  $\delta_0$ :

$$\delta_{\rm env} \approx -\delta_{\rm corr} + \delta_0 = -\alpha V_{\rm corr} + \delta_0$$
 (8)

# 4 Experimental results

In the early night of October 26, 2017, we recorded the interferometric error signal  $\varepsilon$  and correction signal  $V_{\rm corr}$  as a function of time. Due to the limited span of the OPD correction, each time when the required correction became greater than the maximum correction the PZT actuator could provide, the system got uncontrolled

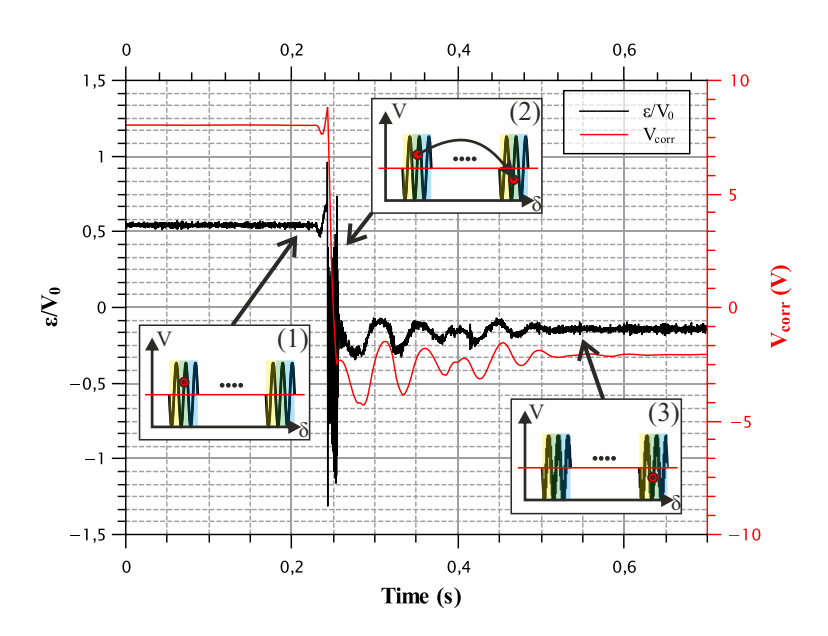


**Fig. 5** Interferometric and error signal during an instability due to the limited span of the OPD correction. When the needed correction exceeds the span of the PZT actuator (1) the system jumps to another operating point (2) before stabilising again (3)



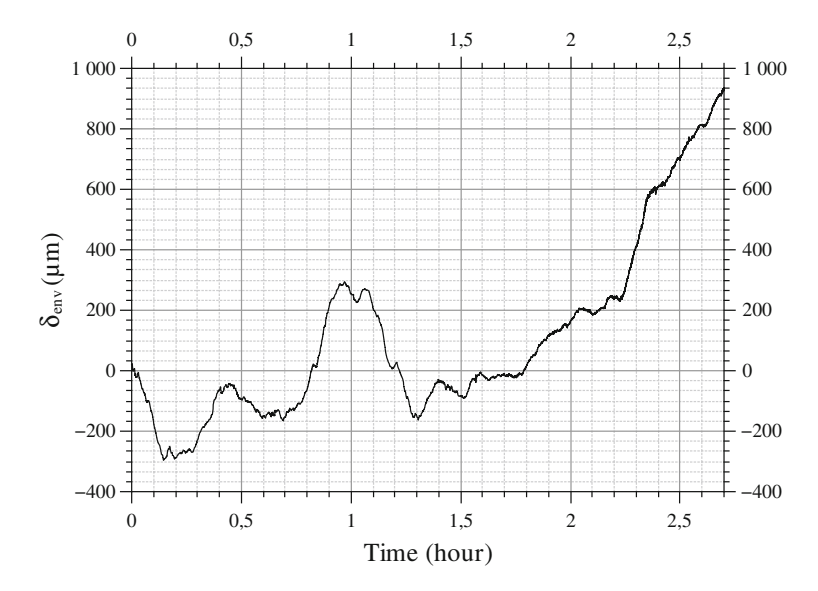


Fig. 6 OPD drift due to the environment  $\delta_{env}$  reconstructed from the correction signal over 2 hours and 45 min. The peak to valley perturbation is equal to 1.2 mm (775  $\lambda$ )

for a few hundreds of milliseconds before automatically stabilising again around the neutral position ( $\delta_{corr} = 0$  nm) of the PZT actuator (see Fig. 5). This transient corresponds to a jump from one set-point, as defined in Fig. 4, to another, several stability zones further. During the 2 hours and 45 min of data acquisition we observed such transient 53 times. However, the aggregate duration of all these uncontrolled periods corresponded to 10 s which represented only 0.1% of the total acquisition time. Equation (8) allows us to reconstruct the OPD drift  $\delta_{env}$ , within the bandwidth of the servo

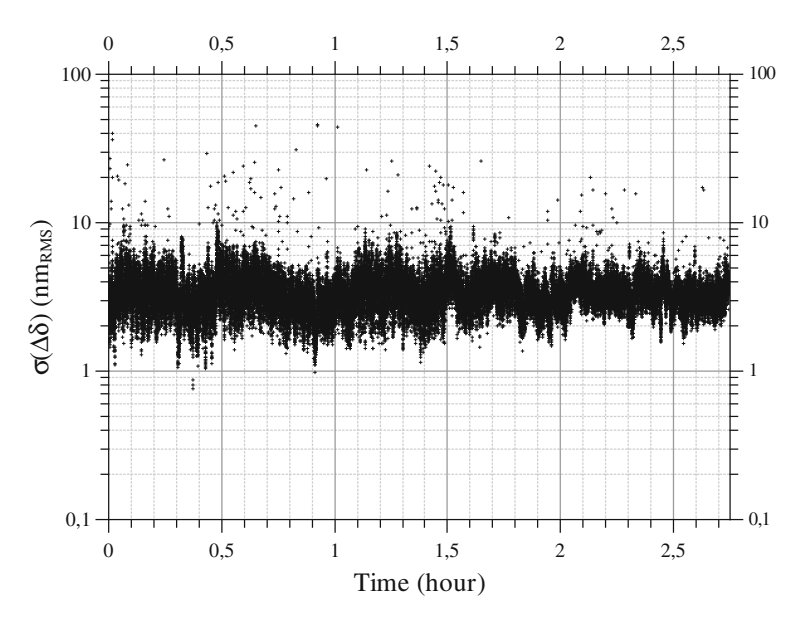
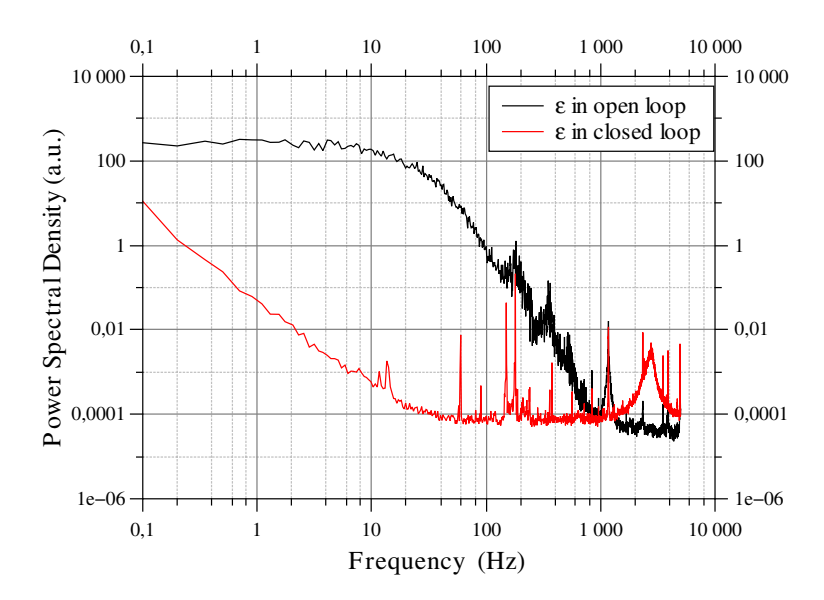


Fig. 7 Standard deviation of the residual OPD  $\Delta\delta$  over 2 h and 45 min. Each point corresponds to a period of 200 ms. The average residual OPD is  $3.4\pm1.3~\mathrm{nm_{RMS}}$  with a stability better than  $5.2~\mathrm{nm_{RMS}}$  for 95% of the frames





**Fig. 8** Power Spectral Density of the error signal in open and closed loop. The servo loop corrects disturbance below 1 kHz up to -60 dB but generates a resonance peak at 2.5 kHz

loop, from the recorded correction signal  $V_{\rm corr}$ . The drift of the OPD due to environmental conditions was continuous and varied slowly as compared to the duration of the uncontrolled periods. These uncontrolled periods were removed by concatenating together the stable periods head to tail. Figure 6 shows the reconstructed drift of the OPD  $\delta_{\rm env}$  as a function of time during the whole experiment. The peak to valley perturbation was equal to 1.2 mm (775  $\lambda$ ).

Using (5), we could also deduce the value of the uncorrected OPD  $\Delta\delta$  from the measure of the error signal  $\varepsilon$ . Figure 7 shows the evolution of the standard deviation of the uncorrected OPD  $\Delta\delta$  as a function of time, integrated over periods of 200 ms (typical coherence time of the atmosphere at Mount Wilson Observatory). The uncontrolled periods were removed from this analysis. The OPD of the interferometer reached an average stability of  $3.4\pm1.3$  nm<sub>RMS</sub> ( $\lambda/450$ ) with a stability better than 5.2 nm<sub>RMS</sub> ( $\lambda/300$ ) for 95% of the frames.

The bandwidth of the correction can be estimated by comparing the power spectral density (PSD) of the error signal in closed and open loop (Fig. 8). The system corrected perturbations below 1 kHz up to -60 dB but a resonance frequency around 2.5 kHz appeared on the error signal PSD. This resonance, due to the non-optimal PID coefficients, corresponded to about 50% of the residual OPD variations.

# 5 Conclusion and perspectives

In this paper, we have described an implementation of a stabilised outdoor hectometric interferometer compliant with astronomical interferometry. The peak-to-valley variation of the OPD did not exceed two millimetres over 2 h and 45 min. We managed to obtain an average stability of  $\lambda/450$  over the same duration. These results are fully compliant with any interferometric application and are encouraging steps



toward the implementation of ALOHA with fibre linkages at the CHARA Array. The first improvement of this experiment will consist in increasing the span of the correction actuator, in order to eliminate the intermittent instability observed in this experiment. This can be done by adding a second stage of correction focused on the compensation of the low frequency and high amplitude perturbations. A motorised fibre delay line with a stroke of a few centimetres can be easily added to the interferometer. In its current form, the PID regulator shows both static errors and a frequency resonance around 2.5 kHz, but it can be significantly improved.

The next step will be to measure fringe contrast of a faint broadband source while stabilising the OPD with the laser signal [12].

**Acknowledgments** This work has been financially supported by the Institut National des Sciences de l'Univers (INSU), the Centre National d'Études Spatiales (CNES) and Thales Alenia Space. We also thank all the OHANA team for lending the optical fibre. The CHARA Array of Georgia State University is supported by the National Science Foundation.

# References

- Scott, N.J., Millan-Gabet, R., Lhomé, E., Ten Brummelaar, T.A., Coudé Du Foresto, V., Sturmann, J., Sturmann, L.: J. Astron. Instrum. 02(2), 1340005 (2013). https://doi.org/10.1142/S225117171340 0059; http://www.worldscientific.com/doi/abs/10.1142/S2251171713400059. 00003
- Petrov, R.G., Malbet, F., Weigelt, G., Antonelli, P., Beckmann, U., Bresson, Y., Chelli, A., Dugué, M., Duvert, G., Gennari, S., Glück, L., Kern, P., Lagarde, S., Le Coarer, E., Lisi, F., Millour, F., Perraut, K., Puget, P., Rantakyrö, F., Robbe-Dubois, S., Roussel, A., Salinari, P., Tatulli, E., Zins, G., Accardo, M., Acke, B., Agabi, K., Altariba, E., Arezki, B., Aristidi, E., Baffa, C., Behrend, J., Blöcker, T., Bonhomme, S., Busoni, S., Cassaing, F., Clausse, J.M., Colin, J., Connot, C., Delboulbé, A., Domiciano de Souza, A., Driebe, T., Feautrier, P., Ferruzzi, D., Forveille, T., Fossat, E., Foy, R., Fraix-Burnet, D., Gallardo, A., Giani, E., Gil, C., Glentzlin, A., Heiden, M., Heininger, M., Hernandez Utrera, O., Hofmann, K.H., Kamm, D., Kiekebusch, M., Kraus, S., Le Contel, D., Le Contel, J.M., Lesourd, T., Lopez, B., Lopez, M., Magnard, Y., Marconi, A., Mars, G., Martinot-Lagarde, G., Mathias, P., Mège, P., Monin, J.L., Mouillet, D., Mourard, D., Nussbaum, E., Ohnaka, K., Pacheco, J., Perrier, C., Rabbia, Y., Rebattu, S., Reynaud, F., Richichi, A., Robini, A., Sacchettini, M., Schertl, D., Schöller, M., Solscheid, W., Spang, A., Stee, P., Stefanini, P., Tallon, M., Tallon-Bosc, I., Tasso, D., Testi, L., Vakili, F., von der Lühe, O., Valtier, J.C., Vannier, M., Ventura, N.: Astron. Astrophys. 464(1), 1 (2007). https://doi.org/10.1051/0004-6361:20066496; http://www.aanda.org/10.1051/0004-6361:20066496
- Monnier, J.D., Berger, J.P., Millan-Gabet, R., ten Brummelaar, T.A. In: Traub, W.A. (ed.) New Frontiers in Stellar Interferometry, vol. 5491, p. 1370 (2004). https://doi.org/10.1117/12.550804. http://proceedings.spiedigitallibrary.org/proceeding.aspx?doi=10.1117/12.550804
- Gillessen, S., Eisenhauer, F., Perrin, G., Brandner, W., Straubmeier, C., Perraut, K., Amorim, A., Schöller, M., Araujo-Hauck, C., Bartko, H. In: Optical and Infrared Interferometry II, vol. 7734, p. 77340Y. International Society for Optics and Photonics (2010)
- Foresto, V.C.d.: Symp. Int. Astron. Union 158, 261 (1994). https://doi.org/10.1017/S0074180900107
   https://www.cambridge.org/core/journals/symposium-international-astronomical-union/article/integrated-optics-in-astronomical-interferometry/11E16D425B164A96835AA43EE8D9AAAB
- Perrin, G., Woillez, J., Lai, O., Guérin, J., Kotani, T., Wizinowich, P.L., Mignant, D.L., Hrynevych, M., Gathright, J., Léna, P., Chaffee, F., Vergnole, S., Delage, L., Reynaud, F., Adamson, A.J., Berthod, C., Brient, B., Collin, C., Crétenet, J., Dauny, F., Deléglise, C., Fédou, P., Goeltzenlichter, T., Guyon, O., Hulin, R., Marlot, C., Marteaud, M., Melse, B.T., Nishikawa, J., Reess, J.M., Ridgway, S.T., Rigaut, F., Roth, K., Tokunaga, A.T., Ziegler, D.: Science 311(5758), 194 (2006). https://doi.org/10.1126/science.1120249; http://science.sciencemag.org/content/311/5758/194



- 7. Woillez, J., Lai, O., Perrin, G., Reynaud, F., Baril, M., Dong, Y., Fédou, P.: Astron. Astrophys. **602**, A116 (2017). https://doi.org/10.1051/0004-6361/201730500. https://www.aanda.org/articles/aa/abs/2017/06/aa30500-17/aa30500-17.html
- 8. Monnier, J.D., Kraus, S., Buscher, D., Berger, J.P., Haniff, C., Ireland, M., Labadie, L., Lacour, S., Le Coroller, H., Petrov, R.G., Pott, J.U., Ridgway, S., Surdej, J., ten Brummelaar, T., Tuthill, P., van Belle, G.: In: Optical and Infrared Interferometry IV, vol. 9146, p. 914610 (2014) https://doi.org/10.1117/12. 2057262
- Brummelaar, T.A.t., McAlister, H.A., Ridgway, S.T., Bagnuolo, J.W.G., Turner, N.H., Sturmann, L., Sturmann, J., Berger, D.H., Ogden, C.E., Cadman, R., Hartkopf, W.I., Hopper, C.H., Shure, M.A.: Astrophys. J. 628(1), 453 (2005). https://doi.org/10.1086/430729; http://iopscience.iop.org/ 0004-637X/628/1/453
- Szemendera, L., Grossard, L., Delage, L., Reynaud, F.: Month. Notic. R. Astron. Soc. 468(3), 3484 (2017). https://doi.org/10.1093/mnras/stx780; https://academic.oup.com/mnras/article-lookup/doi/10.1093/mnras/stx780
- Lehmann, L., Darré, P., Boulogne, H., Delage, L., Grossard, L., Reynaud, F.: Month. Notic. R. Astron. Soc. 477(1), 190 (2018). https://doi.org/10.1093/mnras/sty648; http://academic.oup.com/mnras/article/477/1/190/4925913
- 12. Reynaud, F., Alleman, J.J., Connes, P.: Appl. Opt. **31**(19), 3736 (1992). https://doi.org/10.1364/AO. 31.003736; https://www.osapublishing.org/abstract.cfm?uri=ao-31-19-3736

**Publisher's note** Springer Nature remains neutral with regard to jurisdictional claims in published maps and institutional affiliations.

